Title

Perovskite-related hybrid noble metal iodides: Formamidinium platinum iodide [(FA) 2 Pt IV I 6] and mixed-valence methylammonium gold iodide [(MA) 2 Au I Au III I 6]

Journal

Inorganica Chimica Acta, 468

ISSN

00201693

Authors

Evans, Hayden A
Schueller, Emily C
Smock, Sara R
et al.

Publication Date

2017-11-01

DOI

10.1016/j.ica.2017.04.060

Peer reviewed

Perovskite-Related Hybrid Noble Metal Iodides: Formamidinium Platinum Iodide $[(FA)_2Pt^{IV}I_6]$ and Mixed-Valence Methylammonium Gold Iodide $[(MA)_2Au^{I}Au^{III}I_6]$

Hayden A. Evans,[*,†,‡] Emily C. Schueller,[‡] Sara R. Smock,[†] Guang Wu,[†] Ram Seshadri,[*,‡] and Fred Wudl[*,¶]

†*Department of Chemistry and Biochemistry, University of California Santa Barbara, California 93106, United States*

‡*Materials Research Laboratory, University of California Santa Barbara, California 93106, United States*

¶*Materials Department, University of California Santa Barbara, California 93106, United States*

E-mail: hevans@mrl.ucsb.edu; seshadri@mrl.ucsb.edu; wudl@chem.ucsb.edu

Abstract

Noble metal halide compounds are an exciting class of materials which display unique crystal chemistry with temperature and pressure. Here we report two new compounds, Single-valence formamidinium platinum iodide [$(FA)_2Pt^{IV}I_6$] and mixed-valence methylammonium gold iodide [$(MA)_2Au^{I}Au^{III}I_6$]. Structural changes between 300 K and 100 K have been monitored. The compounds crystallize in two different perovskite-related structure classes, with the added complexity of a disordered, "tumbling", organic cation at 300 K. This tumbling is significantly reduced at 100 K. $(FA)_2Pt^{IV}I_6$ undergoes in-phase octahedral tilting similar to related vacancy-ordered perovskite materials. At 100 K, $(MA)_2Au^{I}Au^{III}I_6$ undergoes a transition which facilitates stronger Au–I covalent bonding as made evident by a contraction of the unit cell and distances between Au and I atoms in the ab plane.

1. Introduction

Noble metal chemistry is exceedingly impactful and relevant, from catalysis to biomedical research.[1] These elements are interesting in that they can provide selective reactivity as well as low activation barriers for oxidation and reduction. Furthermore, noble metal salts and oxides frequently display unique electrical properties owing to the propensity of the noble metal to occur in more than one oxidation state (mixed-valence). Mixed-valence platinum and gold complexes have been studied as one dimensional metallic conductors.[2]

Though the class of mixed-valence alkali and hybrid platinum halide materials have been studied before,[3] the mixed-valence alkali gold halide complexes $A_2[Au^{I}X_2][Au^{III}X_4]$ (A = K, Rb, Cs; X = Cl, Br, I), referred to as $A_2Au_2X_6$ compounds hereafter, have received more attention. These materials were first prepared and described crystallographically in 1979[4] as chloride and bromide derivatives[5] and later as iodides.[6] These materials crystallize with both linear $Au^{I}I_2^-$ and square-plane $Au^{III}I_4^-$ subunits, or alternatively described, as a distorted perovskite structure of elongated and compressed AuI_6 octahedra that stack

alternatively along the [001] and [110] directions. Under pressure, these materials undergo a phase transition to a cubic perovskite structure (stabilizing the Au(II) ion), where the structure of $Cs_2Au_2Cl_6$ above 12.5 GPa and at room temperature undergoes a transition from the tetragonal $I4/mmm$ space group to the cubic $Pm\bar{3}m$,[7] and $Cs_2Au_2I_6$ undergoes a transition from $I4/mmm$ to either $Immm$ or $Ibmm$.[8] As pressure is increased, these $Au^{I}I_6$ and $Au^{III}I_6$ octahedra are driven closer to equivalency, and when equivalent, the electronic structure of Au nears the d^9 valence state. Just beneath the phase transition pressure, strong electron-phonon interactions are due to the mixed-valence effect of the Au (which is understood to be fluctuating rapidly), whereas just above the transition, the strong electron-phonon interactions arise from the Jahn-Teller effect.[9] This phenomenon is undoubtedly of scientific interest, especially for studying the interactions of itinerant electrons and the implications of high pressure on conductivity.

Other hybrid organic-inorganic gold iodides have been prepared previously with univalent Au,[10] as well as a more recent report of two mixed-valence gold iodide compounds made with the counter cations $(NH_3(CH_2)_7NH_3)^{2+}$ and $(NH_3(CH_2)_8NH_3)^{2+}$ which stabilize two dimensional mixed-valence Au-I layers similar to the alkali gold iodides.[11] These compounds are exciting as potential superconductors, as well as potential members of the flourishing hybrid perovskite and perovskite related optoelectronic field.[12] In this report we describe the high and low temperature structures of two hybrid compounds: a vacancy-ordered double perovskite formamidinium platinum iodide $[(FA)_2PtI_6]$ and a mixed-valence methylammonium gold iodide $[(MA)_2Au_2I_6]$. We describe the structural changes that occur with temperature, which are relevant to future high pressure studies of these materials, as well as to related hybrid perovskite optoelectronic material research that is focused on the dynamics of the small organic cations and their implication on device performance.

2. Experimental

Formamidinium iodide ($CH(NH_2)_2I$) was prepared by combining formamidine acetate with hydroiodic acid. Solid formamidine acetate (1.00 eq, 99%, Sigma-Aldrich) was added to room temperature hydroiodic acid (2.0 eq., 57% wt/wt in aqueous solution, Spectrum.) After stirring for 2 hours, the excess solvent was removed using a rotary evaporator. The residue was washed with boiling toluene to remove any triazine contaminant, recrystallized from ethanol, vacuum filtered and dried to give white needle habit crystals. The crystals were placed in a vial wrapped in aluminum foil and stored in a glove box.

Methylammonium iodide (CH_3NH_3I) was prepared following an acid-base reaction of hydroiodic acid with methylamine. A solution of CH_3NH_2 (1.00 eq. 33% wt/wt solution in absolute ethanol, Spectrum) was added to a 0 °C solution of hydroiodic acid (1.05 eq., 57% wt/wt in aqueous solution, Spectrum). After stirring for 2 hours at 0 °C, the excess solvent was removed using a rotary evaporator. The residue was recrystallized twice from a hot ethanol/water mixture, washed with ether, and dried under vacuum overnight to give white, plate habit crystals. The crystals were placed in a vial wrapped in aluminum foil and stored in a desiccator.

The $(FA)_2PtI_6$ was prepared by dissolving 100 mg (0.376 mg) of $PtCl_2$ (Strem, 99.9) in 3.0 g (13 mol HI) fresh 57% wt/wt hydroiodic acid (Spectrum). The hydroiodic acid used contained free iodine due to absence of stabilizer. After dissolution, 84.21 mg (0.752 mmol) of $CH(NH_2)_2I$ was added, prompting formation of a dark precipitate. The solution was brought to a boil, held for 10 minutes, and slowly cooled. Dark cubes of $(FA)_2PtI_6$ were washed with ether, isolated via vacuum filtration, and stored in a glove box. Pt(II) is oxidized to Pt(IV) by the free iodine present in the stabilizer-free hydroiodic acid used in the synthetic procedure.

The $(MA)_2Au_2I_6$ was prepared by dissolving 100 mg (0.254 mmol) $HAuCl_4$ (Strem, 99.9985%) in 3.0 g (13 mol HI) 57% wt/wt hydroiodic acid (Spectrum). The hydroiodic acid used contained free iodine due to absence of stabilizer. After dissolution, 56.86 mg

(0.5078 mol) CH_3NH_3I solid was added, prompting a dark precipitate to form. The solution was brought to a boil and slowly cooled. Dark colored, plates of $(MA)_2Au_2I_6$ form, which were isolated via filtration. $(MA)_2AuI_6$ is very hygroscopic and soluble in most solvents such as ethanol and ether. Single crystals were kept in the hydroiodic acid mother liquor and removed just prior to the diffraction data collection. Crystals of $(MA)_2Au_2I_6$ were flushed with nitrogen during the diffraction experiments.

Single crystal X-ray diffraction data of the title compounds were collected on a Bruker KAPPA APEX II diffractometer equipped with an APEX II CCD detector using a TRIUMPH monochromator with a Mo Kα X-ray source (λ = 0.71073 Å). The crystals were mounted on a cryoloop under Paratone-N oil and kept under nitrogen. Absorption correction of the data was carried out using the multiscan method SADABS.[13] Subsequent calculations were carried out using SHELXTL.[14] Structure determination was done using intrinsic methods. All hydrogen atom positions were omitted. Structure solution, refinement, and creation of publication data was performed using SHELXTL. Crystal structures were prepared using the VESTA software suite.[15]

3. Results and Discussion

3.1 Crystallographic analysis

Figure 1 shows the 300 K and 100 K structures for $(FA)_2PtI_6$. Figure 1(a) depicts the 300 K structure viewed down the c-axis, and illustrates the isolated PtI_6^{-2} octahedra and disordered formamidinium cations. This structure is the same as K_2PtCl_6 where Pt forms a face-centered cubic lattice with formamidinium ions in the tetrahedral cavities (in place of the potassium ions) corresponding to the $Fm\bar{3}m$ cubic space group.[16] The formamidinium moiety has a reliably placed C atom but disordered N atoms. However, the disorder appears to have partial preferential orientation, or "clicking", as is depicted in Figure1(a). These orientations provide the greatest level of hydrogen bonding between the amine

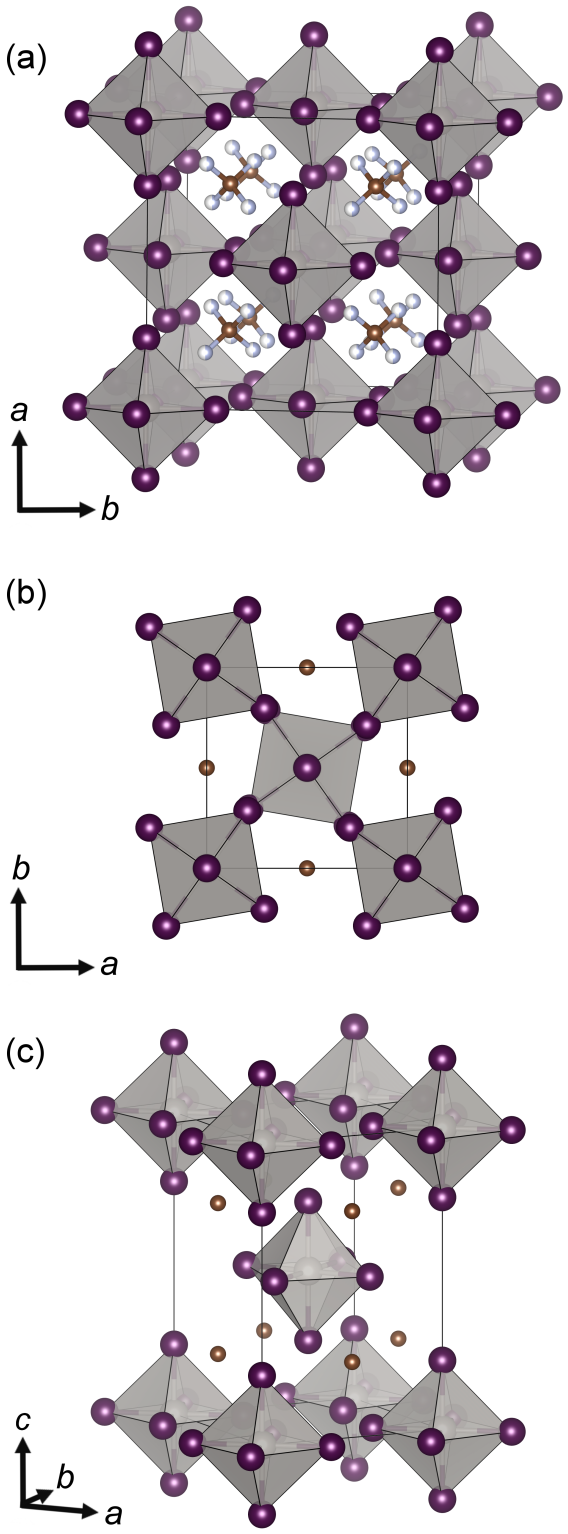

Figure 1: Crystal structure of $(FA)_2PtI_6$. (a) 300 K structure viewed down the c-axis, (b) 100 K, viewed down the c-axis emphasizing octahedral titling and (c) 100 K structure, CCDC submission numbers, RT = 1513695, LT = 1513696.

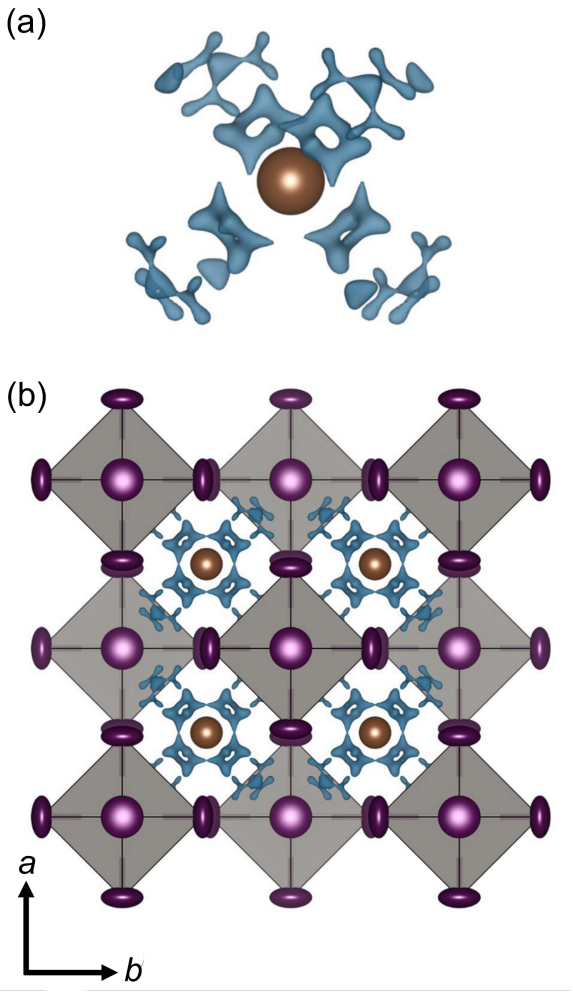

Figure 2: Positive Fourier difference map of 300 K $(FA)_2PtI_6$ structure with 95% probability ellipsoids. The $F(\text{max})(e\mathring{A}^{-3})$ was 1.1059 for this data set, and is displayed with a max level of 0.75. (a) Electron density surrounding carbon atom. (b) Full 300 K structure viewed down the c-axis.

hydrogens and nearest neighbor I atoms. Figure1(b) shows the tetragonal $P4/mnc$ structure at 100 K, where the PtI_6^{-2} octahedra tilt in phase in the ab plane, as is commonly seen in related perovskite and metal vacancy-ordered perovskite structures. The tilting of the vacancy-ordered perovskite, as described by Glazer tilting nomenclature,[17] is $a^0a^0c^+$, meaning that the octahedra rotate in phase equally in the ab plane, and not at all along the c-axis. Figure 1(c) illustrates the structure of $(FA)_2PtI_6$ at 100 K, where the carbon atom is reliably placed. However, in both room and low temperature structures, there was difficulty assigning N density with certainty. To further our understanding of these structures, we determined Fourier difference maps to describe the positive electron density surrounding the formamidinium carbon.

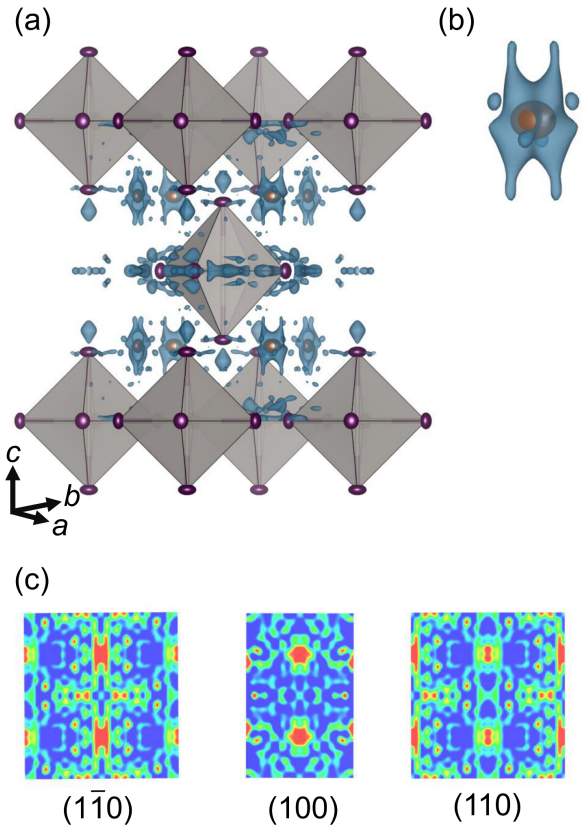

Figure 3: Fourier difference map of the 100 K $(FA)_2PtI_6$ structure with 95% probability ellipsoids. F(max)($e\mathring{A}^{-3}$) was 2.597 for this data set, and is displayed with a max level of 0.97. (a) Full structure. (b) Electron density surrounding carbon. (c) Electron density along the $1\bar{1}0, 100$, and 110 planes. These were chosen to cut the formamidinium carbon atom into 60 degree segments. The two areas of strong density in the center of each plane are the the C atoms, and were purposefully placed for ease of comparison.

In Figure 2(a), it is clear that rings of electron density exist in the form of a tetrahedron, with smaller areas of electron density are observed further out. These densities suggest that on average, the nitrogens of the formamidinium cation are found primarily in one of the four lobes, with the possibility of the formamidinium cation orienting in six different directions. This more predictable behavior is expected when compared to a smaller organic cation methylammonium, which is known to shift and tumble to a greater degree, as we describe later for the $(MA)_2Au_2I_6$ compound. The electron density surrounding the formamidinium carbon in the low temperature structure, on the other hand, is less easily described. Figure 3(a) displays the fourier difference of the full structure, Figure 3(b) the density surrounding the carbon, and Figure 3(c) the electron density along crystallographic planes of interest that intersect the formamidinium carbon atom. The data suggests that the formamidinium cation is statically disordered both in position and orientation as the PtI_6 octahedra tilt, preventing translational symmetry of the N atoms to be reasonably discerned. In Figure 3(b), the oval shaped C ellipsoid and the density surrounding the carbon, leads us to believe that the formamidnium cation can off center substantially without preference during cooling, presenting many possible orientations for the formamidinium cation on average. The electron density maps along the planes of interest agree with this description, as there are many areas of weak electron density which could be attributed to N density. However, as can be inferred from the $1\bar{1}0$ plane, there is observable electron density in the shape of the formamidinium cation (an elongated X shape), which may be a more probable location for the formamidinium cation. The 110 plane suggests that though the carbon and one nitrogen may reside in the same plane, one of the formamidinium nitrogens may not. These many degrees of freedom of the formamidinium cation prevent reliable crystallographic description at low temperature, but when compared to the alkali cation containing vacancy-ordered double perovskites, the polar formamidinium cation provides potentially accessible properties like ferroelectricity, if the material were aligned with an electric field. This warrants future temperature and electric field depen-

dent studies. Furthermore, we expect pressure-induced structural changes to be another area of exploration, similar to work done for comparable vacancy-ordered palladium iodide double perovskites.[18]

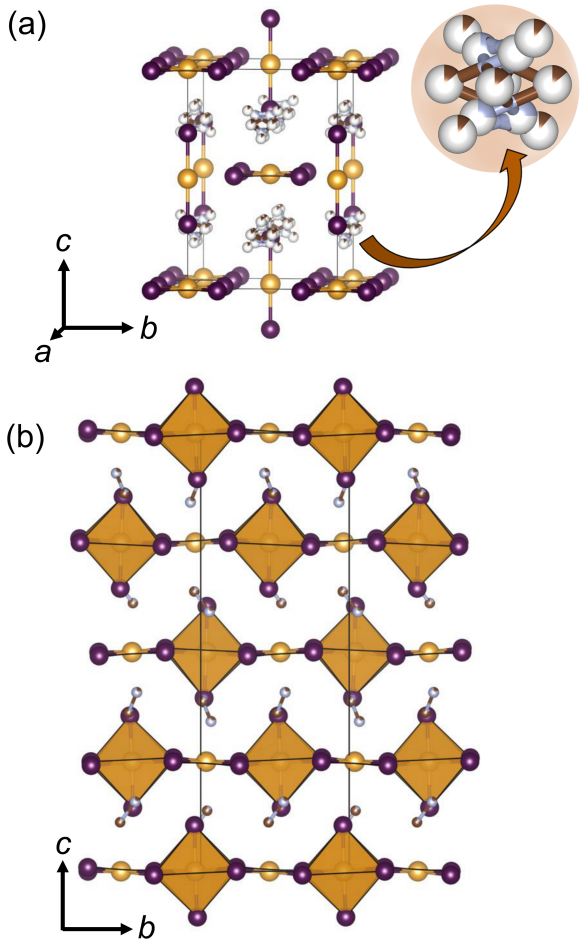

Figure 4: Crystal structure of $[(MA)_2Au^{I}Au^{III}I_6]$. (a) 300 K, emphasizing that at room temperature, the structure is best described as discrete subunits of AuI_2^- and AuI_4^-. An additional view of the disordered methylammonium cation is also included . The bond length between Au and I is upper bound at 3.3 Å. (b) 100 K, viewed down the a-axis emphasizing the now slight tilting of the Au–I octahedra and square planes. The upper bound bond length remains 3.3 Å, indicating that there is increased extended Au–I covalent bonding in the ab plane. CCDC deposition numbers, RT = 1513697, LT = 1513698.

Figure 4 depicts the crystal structure of $(MA)_2Au_2I_6$ at 300 K and 100 K. Figure 4(a) and (b) show the tetragonal $I4/mmm$ room temperature structure, and the low-temperature $P4_32_12$ structure viewed down the a-axis, respectively. The structure of $(MA)_2Au_2I_6$ at

room temperature contains discrete subunits of AuI_2^- and AuI_4^- in addition to considerably disordered methylammonium cations. Much like the modeling that has described methylammonium in methylammonium lead iodide ($MAPbI_3$),[19] it is clear that the cation is tumbling within its cavity, changing orientation rapidly as it hydrogen bonds between one of the twelve nearest neighbor iodide atoms. This is possible due to the low energy barrier for the cation to shift.[20] Interestingly, the structure of $(MA)_2Au_2I_6$ at low temperature, Figure 4(b), undergoes a distortion which forms buckled Au-I sheets. This suggests that the structure at low temperatures has increased covalent bonding between the Au of the AuI_2^- subunits and the neighboring I of the AuI_4^- moieties. Prior reports have described that the bonding between gold and iodine is analogous to polyiodides due to similar electronegativities of Au and I (2.54 and 2.66, respectively),[21] with the AuI_2 subunit directly comparable with the linear I_3^- anion. If we apply the same criteria for determining covalent bonding, where the I–I bonding distance is upper bound at 3.3 Å, then at 100 K sheets of Au–I square planes and octahedra form infinitely in the ab plane, as is depicted in Figure 4(b). In regards to the methylammonium cation at low temperature, the structure was solved with a translational symmetry describing the orientation of the methylammonium cation but with understandable difficulty in distinguishing between the nitrogen or carbon atoms of the methylammonium. This is due to low Z contrast. It could be quite similar to methylammonium lead iodide where orientation of the methylammonium cation alternates consistently but this is hard to discern.[22]

4. Conclusion

The structures of the vacancy-ordered double perovskite $(FA)_2PtI_6$ and the mixed-valence $(MA)_2Au_2I_6$ are reported at 300 K and 100 K. At 300 K, the structure of $(FA)_2PtI_6$ can be described with the cubic space group $Fm\bar{3}m$, and at 100 K with the tetragonal space group $P4/mnc$. This reduced symmetry is caused by in-phase tilting of the discrete Pt–I octa-

Table 1: Crystallographic information for title compounds

Empirical formula	$(MA)_2Au_2I_6$	$(MA)_2Au_2I_6$	$(FA)_2Pt^{IV}I_6$	$(FA)_2Pt^{IV}I_6$
Diffractometer	Bruker KAPPA APEX II			
Monochrometer	TRIUMPH			
mode	Omega scan			
Temperature (K)	300	100	300	100
Crystal habit, color	Plate, gold		Cube, black	
Crystal system	Tetragonal	Tetragonal	Cubic	Tetragonal
Space group	$I4/mmm$ (No. 139)	$P4_32_12$ (No. 96)	$Fm\bar{3}m$ (No. 225)	$P4/mnc$ (No. 128)
Volume (Å^3)	895.8(2)	1720.1(2)	1401.8(2)	674.65
a (Å)	8.490(7)	8.3513(4)	11.192(5)	7.6428(5)
b (Å)	8.490(7)	8.3513(4)	11.192(5)	7.6428(5)
c (Å)	12.428(9)	24.663(2)	11.192(5)	11.6659(7)
Z	2	4	4	2
ρ (g mol^{-1})	1213.42	1213.42	1046.63	1046.63
Dens. (g cm^{-3})	4.521	4.686	4.959	4.906
Abs. (mm^{-1})	26.669	27.776	23.193	23.870
F_{000}	1028	2032	1784	872
2θ range	2.906 to 27.028	2.575 to 27.039	3.153 to 30.533	3.187 to 25.242
Reflections (Unique)	2018(299)	10354 (1887)	1032 (144)	687 (394)
R_{int}	0.0551	0.0529	0.0390	0.0155
Final R_1, wR_R $[I > 2\sigma(I)]$	0.0396, 0.1139	0.0469, 0.0870	0.0507, 0.1074	0.0266, 0.0530
R_1, wR_R, (all data)	0.0433, 0.1159	0.0469, 0.0900	0.0507, 0.1074	0.0269, 0.0531
∂F ($e\mathring{A}^{-3}$)	2.068 and -1.742	4.457 and -2.101	1.082 and -5.908	1.806 and -2.955
GOF	1.246	1.074	1.291	1.348

hedra. This tilting is seen in the related and well-studied K_2PtCl_6 compound, as well as other similar vacancy-ordered double perovskite compounds. The $(FA)_2PtI_6$ material at 300 K has a predictably disordered formamidinium cation. At 100 K, the formamidinium cation presents static disorder, preventing accurate assignment of the formamidinium N atoms. Due to the polar nature of the formamidinium cation, future temperature and electric field-dependent studies are of interest to examine induced polarization of the material. The $(MA)_2Au_2I_6$ material crystallizes in the tetragonal space group of $I4/mmm$ at room temperature, and in the tetragonal space group $P4_32_12$ at low-temperature. This compound contains discrete AuI_2^- and AuI_4^- subunits at room temperature, but upon cooling, an increased Au–I covalent bonding pattern occurs in the ab plane, producing buckled Au–I sheets. Due to the similar electronegativities of Au and I, this material at 100 K can be viewed as an extended polyiodide analogue. Additionally, like the related alkali metal compounds, we expect $(MA)_2Au_2I_6$ to display interesting crystal chemistry under pressure, forming a cubic perovskite and stabilizing the electronically interesting Au(II) ion.

Acknowledgments

This work was supported by the U.S. Department of Energy, Office of Science, Basic Energy Sciences under award number DE-SC-0012541. The research involved the use of shared experimental facilities of the Materials Research Laboratory at UCSB supported by the MRSEC Program of the National Science Foundation under Award No. DMR 1121053. We would like to thank Dr. Geneva Laurita for fruitful discussions.

References

(1) a) M. C. Gimeno, The Chemistry of Gold, Wiley-VCH, Weinheim, 2009, 1–63; b) F. R. Hartley, The Chemistry of Platinum and Palladium, Wiley, New York, 1973 ; c) L. R. Kelland, N. P. Far-

rell, Platinum-Based Drugs in Cancer Therapy, Humana Press: Totawa, 2000; d) M. Albrecht, G. Martin van Koten, *Angew. Chem. Int. Ed.* **2001**, *40*, 3750–3781.

(2) a) F. Mehran, B. A. Scott, *Phys. Rev. Lett.* **1973**, *31*, 1347–1350; b) J. M. Williams, *Adv. Inorg. Chem.*, **1983**, *26*, 235–268 and references therin; c) K. Uemura, K. Fukui, K. Yamasaki, K. Matsumoto, M. Ebihara, *Inorg. Chem.* **2010**, *49*, 7323–7330; d) C. H. Hendon, A. Walsh, N. Akiyama, Y. Konno, T. Kajiwara, T. Ito, H. Kitagawa, K. Saki, *Nat. Commun.* **2016**, *7*, 1–6.

(3) a) G. Thiele, D. Wagner, *Z. Anorg. Allg. Chem.* **1978**, *446*, 126–130 ; b) G. Thiele, C. Mrozek, D. Kammerer, K. Wittmann, *Z. Naturforsch.* **1983**, *38b*, 905–910; c) G. Thiele, H. W. Rotter, W. Bächle, *Z. Anorg. Allg. Chem.* **1989**, *572*, 55–62; d) W. Baechle, H. W. Rotter, G. Thiele, R. J. H. Clark, *Inorg. Chim. Acta.* **1992**, *191*, 121–129; e) G. Thiele, H. W. Rotter, W. Bächle, *Z. Anorg. Allg. Chem.* **1994**, *620*, 1271–1277.

(4) a) J. Strähle, J. Gelinek, J. Kölmel, *Z. Anorg. Allg. Chem.* **1979**, *41*, 241–260; b) J. Strähle, J. Gelinek, J. Kölmel, A. M. Nemecek, *Z. Naturforsch. B Chem. Sci.* **1979**, *34*, 1047–1052.

(5) a) N. Matsushita, H. Kitagawa, N. Kojima, *Acta Crystallogr. Sect. C-Cryst. Struct. Commun.* **1997**, *53*, 663666; b) S. C. Riggs, M. C. Shapiro, F. Corredor, T. H. Geballe, I. R. Fisher, G. T. McCandless, J. Y. Chan, *J. Cryst. Growth* **2012**, *355*, 13–16.

(6) a) H. Tanino, K. Takahashi, *Solid State Commun.* **1986**, *59*, 825–827; b) H. Kitagawa, N. Kojima, T. Nakajima, *J. Chem. Soc. Dalton. Trans*, **1991**, *11*, 3121–3125; c) N. Kojima, A. Tanaka, H. Sakai, Y, Maeda, *Nucl. Instr. Method. Phys. Res.*, **1993**, *B76*, 366–367; d) K. Ikeda, N. Kojima, Y. Ono, Y. Kobayashi, M. Seto, X. J. Liu, Y. Moritomo, *Hyperfine Interact.* **2004**, *154*, 1–4.

(7) N. Matsushita, H. Ahsbahs, S. S. Hafner, N. Kojima, *Rev. High Pressure Sci. Technol.* **1998**, *7*, 329–331.

(8) S. Wang, S. Hirai, M. C. Shapiro, S. C. Riggs, T. H. Geballe, W. L. Mao, I. R. Fisher, *Phys. Rev. B.* **2013**, *87*, 54104-1–54104-6.

(9) H. Kitagawa, N. Kojima, H. Takahashi, N. Mori, *Synth. Metals* **1993**, *56*, 1726–1729

(10) a) P. Braunstein, A. Mueller, H. Boegge, *Inorg. Chem.* **1986**, *25*, 2104–2106; b) J. R. Ferraro, M. A. Beno, R. J. Thorn, H. H. Wang, K. S. Webb, J. M. Williams, *J. Phys. Chem. Solids* **1986**, *47*, 301–308; c) Z. Tang, A. P. Litvinchuk, H.-G. Lee, A. M. Guloy, *Inorg. Chem.* **1998**, *37*, 4752–4753; d) S. D. Gupta, *J. Am. Chem. Soc.* **1914**, *36*, 747–751.

(11) J. Guan, Z. Tang, A. M. Guloy, *Chem. Commun.* **1999**, *18*, 1833–1834.

(12) a) B. Saparov, D. B. Mitzi, *Chem. Rev.* **2016**, *116*, 4558–4596; b) Z. Xu, D. B. Mitzi, *Inorg. Chem. Commun.* **2003**, *42*, 6589–6591; c) D. B. Mitzi, *Inorg. Chem.* **2000**, *39*, 6107–6113; d) A. Kojima, K. Teshima, Y. Shirai, T. Miyasaka, *J. Am. Chem. Soc.* **2009**, *131*, e) G. Kieslich, S. Sun, A. K. Cheetham, *Chem. Sci.* **2015**, *6*, 3430–3433; f) G. Kieslich, S. Sun, A. K. Cheetham, *Chem. Sci.* **2014**, *5*, 4712–4715; g) A. J. Lehner, D. H. Fabini, H. A. Evans, C. A. Hébert, S. R. Smock, J. Hu, H. Wang, J. W. Zwanziger, M. L. Chabinyc, R. Seshadri, *Chem. Mater.* **2015**, *27*, 7137–7148; h) D. H. Fabini, T. Hogan, H. A. Evans, C. C. Stoumpos, M. G. Kanatzidis, R. Seshadri, *J. Phys. Chem. Lett.* **2016**, *7*, 376–381; i) H. A. Evans, A. J. Lehner, J. G. Labram, D. H. Fabini, O. Barreda, S. R. Smock, G. Wu, M. L. Chabinyc, R. Seshadri, F. Wudl, *Chem. Mater.* **2016**, *28*, 3607–3611; j) D. H. Fabini, G. Laurita, J. S. Bechtel, C. C. Stoumpos, H. A. Evans, A. Van der Ven, M. G. Kanatzidis, R. Seshadri, *J. Am. Chem. Soc.* **2016**, *138*, 11820–11832; k) D. H. Fabini, J. G. Labram, A. J. Lehner, J. S. Bechtel, H. A. Evans, A. Van der Ven, F. Wudl, M. L. Chabinyc, R. Seshadri, *Inorg. Chem.*, **2017**, *56*, 11–25

(13) SADABS; Sheldrich, G. M. University of Gottingen: Germany, **2005**.

(14) SHELXTL PC, Version 6.12; Bruker AXS Inc.: Madison, WI, **2005**.

(15) K. Momma, F. Izumi, *Commission on Crystallogr. Comput.* **2006**, *7*, 106–119.

(16) a) P. J. Ewing, L. Pauling, *Z. Kristallogr.* **1928**, *68*, 223230 b) R. J. Williams, D. R. Dillin, W. O. Milligan, *Acta Crystallogr. Sect. B-Struct. Sci.* **1973**, *29*, 1369–1372.

(17) A. Glazer, *Acta Crystallogr. Sect. B-Struct. Sci.* **1972**, *28*, 3384–3392

(18) B. Schüpp, P. Heines, A. Savin, H.-L Keller, *Inorg. Chem.* **2000**, *39*, 732–735

(19) A. M. A. Leguy, J. M. Frost, A. P. McMahon, V. G. Sakai, W. Kockelmann, C. Law, X. Li, F. Foglia, A. Walsh, B. C. Oregan, *Nat. Commun.* **2015**, *6*, 1–10.

(20) C. Quarti, G. Grancini, E. Mosconi, P. Bruno, J. M. Ball, M. M. Lee, H. J. Snaith, A. Petrozza, F. D. Angelis, *J. Phys. Chem. Lett.* **2014**, *5*, 279–284.

(21) a) P. H. Svensson, L. Kloo, *Chem. Rev.* **2003**, *103*, 16491684; b) N. N. Greenwood, A. Earnshaw, *Chemistry of the Elements*, Pergamon Press, New York, **1990**, Chapter 28 c) S. Madhu, H. A. Evans, V. V. T. Doan-Nguyen, J. G. Labram, G. Wu, M. L. Chabinyc, R. Seshadri, F. Wudl, *Angew. Chem. Int. Ed.* **2016**, *55*, 8032–8035.

(22) M. T. Weller, O. J. Weber, P. F. Henry, A. M. Di Pumpo, T. C. Hansen, *Chem. Commun.* **2015**, *51*, 4180–4183.